Catalysis Science & Technology

Accepted Manuscript

This article can be cited before page numbers have been issued, to do this please use: M. Potter, J. Kezina, R. Bounds, M. Carravetta, T. Mezza and R. Raja, *Catal. Sci. Technol.*, 2018, DOI: 10.1039/C8CY01370E.

ROYAL SOCIETY OF CHEMISTRY

rsc.li/catalysis

View Article Online
DOI: 10.1039/C8CY01370E

Journal Name

ARTICLE

Investigating the role of framework topology and accessible active sites in silicoaluminophosphates for modulating acid-catalysis

Received 00th January 20xx,
Accepted 00th January 20xx

DOI: 10.1039/x0xx00000x

www.rsc.org/

Matthew E. Potter,[a]* Julija Kezina,[a] Richard Bounds,[a] Marina Carravetta,[a] Thomas M. Mezza[b] and Robert Raja[a]*

The structure-property correlations, which direct the formation of specific active-acid sites in nanoporous silicoaluminophosphates (SAPOs) have been explored, to afford a molecular basis for the rational design of solid-acid catalysts. It is demonstrated that the influence of the specific zeotype framework extends beyond modulating Brønsted acidity, with the framework topology playing a fundamental role in reaction kinetics. The structural integrity and nature of the active site has been probed using a combined catalysis and multi-technique characterization study, aimed at optimizing the production of ε-caprolactam.

Introduction

Utilising *in situ* spectroscopy for understanding the precise nature and role of active sites at the molecular level, has led to the rational design of single-site heterogeneous catalysts[1-4] for the manufacture of ε-caprolactam, an important precursor in the production of nylon-6.[5] Conventionally, ε-caprolactam is manufactured by the modified Raschig process using oleum and hydroxylamine sulfate, which results in the generation of ammonium sulfate as a by-product.[6,7] With a view to improving the atom economy and energy efficiency, a two-step method was devised[8,9] to transform cyclohexanone to ε-caprolactam. The first step employed TS-1 to activate hydrogen peroxide and ammonia to produce cyclohexanone oxime,[8] while the subsequent Beckmann rearrangement of cyclohexanone oxime is performed in the vapour phase (> 300 °C) with a high-silica ZSM-5 (MFI) catalyst, circumventing the need for oleum and other corrosive mineral acids (Table 1).[9] The environmental benefits of this process prompted a significant body of research into the individual reaction steps, with HZSM-5 being prolific for the Beckmann rearrangement.[9-13] Similarly a range of species have been synthesized with the aim of increasing the lactam yield (Table 1).[14-24]

The Beckmann rearrangement of cyclohexanone oxime has more recently been performed at low temperature, liquid-phase conditions,[15,25,26] achieving near-quantitative yield of ε-caprolactam (> 98 % under optimized conditions) using a SAPO-37 catalyst.[14,15] Zeolite Y, which possesses the same framework topology (FAU) as SAPO-37, on the other hand, leads to much inferior yields of ε-caprolactam (29 mol%, Table 1), under identical conditions.[15] Interestingly, HZSM-5 (while proficient in the gas-phase Beckmann rearrangement), affords inferior catalytic performance in the liquid-phase (21 mol%, Table 1). This is something we attributed to the significantly slower internal diffusion of cyclohexanone oxime in the MFI framework.[15] It is therefore pertinent to identify the precise nature of the active sites within these SAPO frameworks, as this will facilitate meaningful structure-property correlations to be established on the basis of the nature and strength of the solid-acid sites. Contrasting the structural and spectroscopic properties of the SAPO-37 catalyst with zeolitic analogues (Zeolite-Y and ZSM-5) and other SAPO frameworks, will further substantiate the influence of the zeolite/zeotype topology and aid mechanistic insights in the low-temperature Beckmann rearrangement of cyclohexanone oxime.

Table 1 Summary of Beckmann rearrangement methodologies using solid-acid catalysts

Catalyst	Temp/°C	Conv/mol%[a]	Sel/mol%[b]	Ref
HP-SAPO-34[c]	325	99	95	19
Nb_2O_5/SiO_2	325	99	99	20
MFI SiO_2	350	48	5	21
MFI SiO_2 Nanosheet	350	77	92	21
Al-MCM-41	350	76	99	22
ZSM-5	380	99	96	23
MgSiAlPO-5	400	77	70	24
SAPO-37	130	99	98	15
Zeolite-Y	130	99	29	15
ZSM-5	130	47	44	15
Zeolite-Beta	130	54	98	25
Al-MCM-41	130	51	90	26

a) Conversion of cyclohexanone oxime, b) Selectivity to ε-caprolactam; c) Hierarchically Porous (HP).

[a] School of Chemistry, University of Southampton, University Road, Southampton, SO17 1BJ, United Kingdom.
[b] UOP LLC, A Honeywell Company, 25 East Algonquin Road, Des Plaines, IL 60017, USA.

Electronic Supplementary Information (ESI) available: Full experimental details, further characterization data, catalysis data and appropriate references. See DOI: 10.1039/x0xx00000x

While it is possible to engineer different sites in a framework using different dopants,[27-32] it is also possible that one dopant will create diverse acid sites when incorporated into different frameworks. It has previously been shown that Si^{4+} ions doped into both AlPO-5 (AFI) and AlPO-34 (CHA) frameworks will create distinct active sites.[33] When substituted into SAPO-34, Si primarily undergoes type II substitution (Figure S1), this yielding isolated active sites with a higher proportion of strong Brønsted acid sites.[33] Whereas Si in SAPO-5 primarily undergoes a mixture of type II and type III substitution, leading to silicon islanding.[33] This leads to clusters of acid sites, which are typically stronger Brønsted acid sites, than the isolated species within the same framework. As such, the framework topology plays a vital role in regulating the nature and type of the active site. This is highlighted further in our previous work, where we show the benefits of introducing mesoporosity into AlPO systems, generating hierarchical species for the vapour-phase Beckmann rearrangement.[34]

In this work we have chosen to focus on 4 distinct silicon-doped AlPO frameworks, namely AlPO-5, AlPO-34, AlPO-37 and AlPO-41.[35] These architectures were chosen due to the significant variations in pore-size and channel dimensions that exist between the frameworks. Given our previous work in contrasting the catalytic efficacy of different zeolite frameworks (and types of acid site) for the Beckmann rearrangement, we intend to explore the influence of both pore-size and the nature of the acid site in these SAPO frameworks.

The dimensions of the nanoporous cavities present in AlPOs play a prominent role in the Beckmann rearrangement, particularly in the liquid-phase,[36,37] where the precise geometry and orientation of the micropores plays a crucial role in the diffusion of substrates, especially at low-temperatures.[38] While the properties of the framework are important, their influence over active site formation is also very significant. A range of silicon environments (Figure S1) are possible on incorporating silicon into an AlPO framework, each with distinct acidic properties. The subtly different synthetic protocols (Table S1) for each framework often cause a framework to favour a specific silicon site or environment.[39,40] Consequently, a wide range of characterization techniques, to simultaneously probe both the active silicon species and the framework topology are required, before meaningful structure-property correlations can be established.

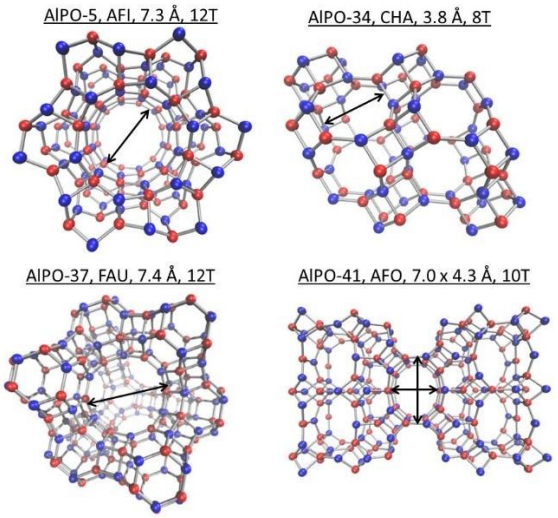

Figure 1 Contrasting pore-apertures in AlPO frameworks.

Results and discussions

The textural properties of the SAPO species were investigated using a range of physico-chemical techniques. Powder X-ray diffraction (XRD) confirmed that in all cases, the desired framework had been exclusively formed. No evidence of phase-impurities or extra-framework species were detected (Figure 2, Table 2). Reitveld analysis yielded unit cell parameters for the different frameworks (Table S2). The structural data were in excellent agreement (< 2% deviation) with the expected values derived from the ideal frameworks,[41] subtle variations are anticipated, given the distortion of isomorphously incorporating silicon into an AlPO framework.[42]

Analysis of silicon content in the SAPO materials confirms the low-levels expected (Table 2 and S3), following the trend SAPO-34 > SAPO-37 >> SAPO-5 > SAPO-41. While it would be desirable to have a consistent silicon loading for all samples, many SAPO species can only be formed, in a phase-pure manner, within a limited silicon content range, thus variations are accepted,[33] with a notable difference between the silicon loading of the two 3-dimensional systems (SAPO-34 and -37) and the one-dimensional species (SAPO-5 and -41). The effect of silicon incorporation was investigated using nitrogen physisorption. In all cases the surface area is in good agreement with the undoped species, with silicon incorporation only subtly lowering the surface area, as observed in previous work (Table 2).[2,30] The chabazite and faujasite frameworks (SAPO-34 and -37, respectively) show characteristically superior surface areas, given the intertwining micropores in these three-dimensional structures.[15,32,43] In all cases the external surface area (Table 2) accounts for between 7 – 13 % of the total surface area. Overall this data was in good agreement with the expected values that have been reported in literature.[2,15,33,35] The SAPO materials show crystalline particles, in the range of 1 – 5 µm, in

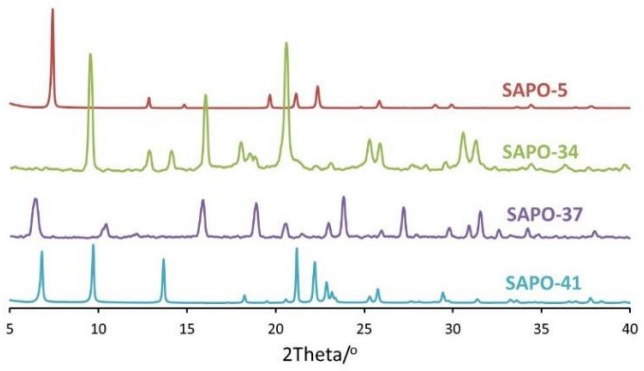

Figure 2 Powder XRD confirming structural purity of different SAPO frameworks.

View Article Online
DOI: 10.1039/C8CY01370F

Table 2 Summary of physical characteristics

Material	Space group	BET Surface area / $m^2 g^{-1}$	T-plot External Surface area / $m^2 g^{-1}$	Si / wt%
SAPO-5	P6cc	271	29	1.4
SAPO-34	R-3m	449	32	3.4
SAPO-37	Fd-3m	588	75	3.0
SAPO-41	Cmcm	316	26	1.1

accordance with the intended space-groups or previously published work (Figure 3 and Table 2).[2,15,33,35,41] This confirms the framework integrity of the synthesized SAPO materials.

One of the primary challenges in heterogeneous catalysis is that the active site is typically a small fraction of the catalyst, shrouded by the host matrix.[44-48] A comprehensive understanding of the active site requires an array of characterization techniques to, directly and indirectly, probe the acidic properties and local environment of the active species. In this vein, we combine findings from magic-angle spinning NMR (MAS NMR), temperature-programmed desorption (TPD) and Fourier-transform infra-red spectroscopy (FT-IR) to establish structure-property correlations that relate to the nature and strength of the acid sites within our solid catalysts.

^{27}Al MAS NMR (Figure S2) of dehydrated samples, shows a prominent signal between 32-36 ppm, which can be attributed to tetrahedrally coordinated framework species, $Al(OP)_4$.[49,50] In some cases this signal is broadened by the presence of penta-coordinated Al species and hydrated $Al(OP)_4(H_2O)_x$ species. There are also signals attributable to octahedral AlO_6 species at ~ 0 ppm.[49,50] ^{31}P NMR (Figure S3) provides complimentary evidence to the ^{27}Al NMR, with all frameworks showing signals within the -25 to -31 ppm range, assigned to the primary $P(OAl)_4$ species.[51,52]

Silicon nuclei in AlPO frameworks are markedly sensitive to neighbouring framework atoms. This can be observed *via* ^{29}Si MAS NMR (Figure 4), with each possible $Si(OAl)_x(OSi)_{4-x}$ species occurring at a distinct chemical shift, allowing them to be readily identified.[51,52] The charge imbalance from silicon undergoing type II substitution (replacing a phosphorus atom), is balanced by a proton binding to an adjacent oxygen atom, generating a Brønsted acid site (Figure S1).[2,15,33] Other silicon environments may also facilitate Brønsted acidity: non-isolated silicon (silicon islands) occur from the combination of type II and type III silicon substitution. Smaller silicon islands (possessing mainly $Si(OAl)_3(OSi)$ groups, more type II substitution) will produce more acidity per silicon atom than larger silicon islands (comprised mainly of $Si(OSi)_4$ environments and type III substitution, Figure S1). When located within the same framework, acid sites from silicon islanding are typically stronger than those from isolated silicon. ^{29}Si MAS NMR (Figure 4) of the faujasitic SAPO-37 and chabazitic SAPO-34 show a dominant feature between –89 and -91 ppm, corresponding to $Si(OAl)_4$, directly associated with Brønsted acidity. These two spectra show no other features, suggesting that silicon predominantly substitutes a phosphorus atom, *via* type II substitution, therefore creating isolated acid sites ($Si(OAl)_4$). In stark contrast, the SAPO-5 and SAPO-41 samples show a signal with a maxima at -97 and -98 ppm respectively. Signals in this region signify the presence of Si-O-Si bonds within the sample, attributed to silicon islanding and diminished site isolation.[39,40,51,52]

While MAS NMR is able to determine the environment of the silicon species, probe-based techniques are required to study the behavior of these silicon sites, in order to contrast the nature and strength of the acid sites. Consequently, probe-based FT-IR and TPD techniques have been employed to accentuate the features of the active species present. FT-IR experiments can simultaneously probe the nature, behavior and location of the acid sites by employing a range of basic probe-molecules, including CO and collidine (2,4,6-trimethylpyridine). Initially the hydroxyl-region (3800 – 3500 cm^{-1}, Figure 5) of the bare-frameworks was observed to focus

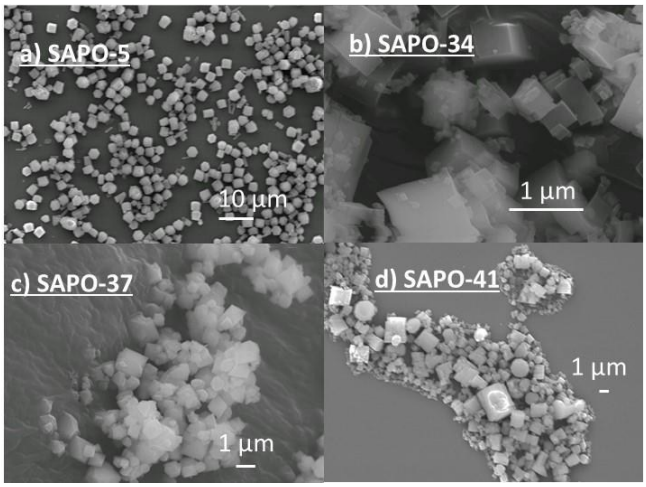

Figure 3 Scanning electron microscopy (SEM) images showing particle morphology that is consistent with literature findings.[2,15,33,35]

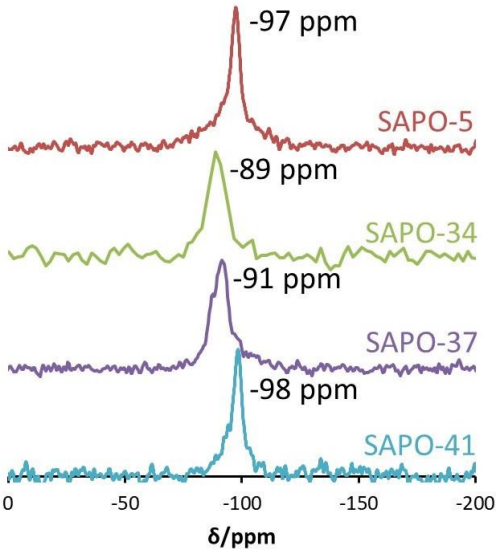

Figure 4 ^{29}Si MAS NMR to probe the local silicon environments, peak maxima shown.

on the protonic species. Subtle features at 3745 and 3678 cm^{-1} were present in all SAPO catalysts,[53] corresponding to Si-OH and P-OH defect species, that are ubiquitous in SAPOs.[53] The frameworks associated with isolated active sites (SAPO-34 and SAPO-37) both show two distinct Si-OH-Al signals, further suggesting isomorphous framework substitution. SAPO-37 shows these peaks at 3640 and 3575 cm^{-1}, representing protons within the supercages and the sodalite cages, respectively.[54] The disparity between the two signals is due to the varying degree of hydrogen bonding the proton experiences with the framework oxygen in the two different conformations. Similarly, SAPO-34 exhibits two proton signals. The signal at 3626 cm^{-1} corresponds to protons within open cages, whereas the signal at 3599 cm^{-1} occurs from protons within the 6-rings of the 6,6 secondary building units.[55] The spectra of the SAPO-5 and SAPO-41 species complement the NMR findings, with the signals corresponding to the framework-substituted silicon species (Si-OH-Al) being less intense (Figure 5). This is in agreement with lower silicon content, a lack of site isolation and silicon islanding observed in the ^{29}Si MAS NMR (Figure 4).

To explore the strength and number of acid sites, CO was employed as a molecular probe. On interacting with CO a decrease in the hydroxyl OH stretches is accompanied by the appearance of a signal in the 3300 – 3500 cm^{-1} region attributed to O-H-CO interactions (Figure 6A, S4 and S5).[54-59] Further, a signal attributed to the CO stretch appears in the 2200 – 2150 cm^{-1} region (Figures 6B, S6 and S7). The OH stretch in the smaller-pore SAPO-34 framework completely diminishes on CO adsorption, indicating all protons are accessible. The two signals which appear in the CO region, (2170 and 2140 cm^{-1}) are attributed to CO adsorbed on Brønsted acid sites, and liquid-like physisorbed CO, respectively.[60] No CO bands were observed above 2190 cm^{-1}, confirming no Lewis acidity. In SAPO-37, the different acidic environments show contrasting behaviour as the signal at 3575 cm^{-1} is present after CO adsorption, suggesting it is inaccessible. However the primary signal at 3641 cm^{-1} significantly diminishes on CO adsorption, showing that a large proportion of the Brønsted acid species in SAPO-37 are accessible. The few acidic protons present in SAPO-5 and SAPO-41 are all accessible to CO, as the OH bands are no longer present after CO adsorption.

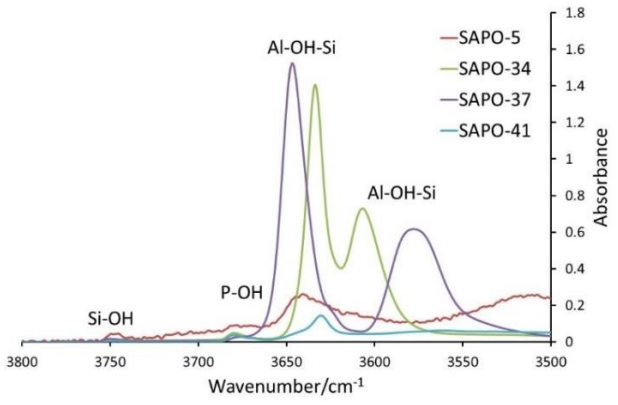

Figure 5 FT-IR spectra highlighting the O-H stretching region of SAPO samples.

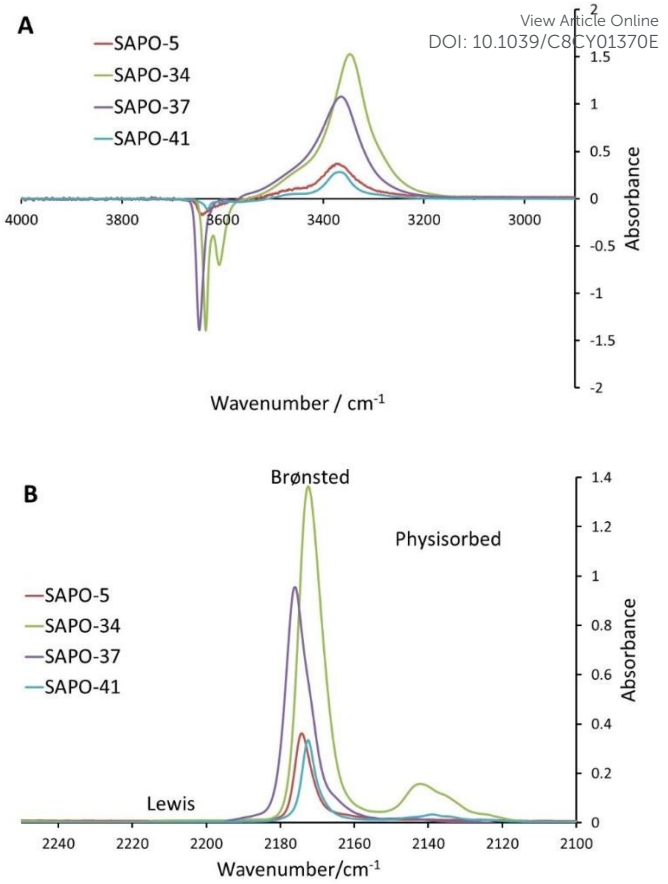

Figure 6 FT-IR spectra after adsorbing 0.18 cm^3 of CO at 100 K, in the hydroxyl (A) and CO stretch (B) regions.

The amount of OH signal shift, after deconvolution, on adsorbing CO, relates to the acid site strength, with stronger acid sites shifting to a larger extent. SAPO-5 shows just one O-H-CO peak, with a shift of just 270 cm^{-1}, corresponding to medium strength sites. SAPO-41 shows two different peaks appearing on CO interaction. The main signal at 3630 cm^{-1}, with a shift of 260 cm^{-1} shows primarily medium strength sites, with some weaker sites present as the peak at 3644 cm^{-1} shifts by just 190 cm^{-1} on CO interaction. The acid sites in SAPO-37 shows a stronger interaction with CO, as one peak appears with a shift of 305 cm^{-1}. In contrast SAPO-34 shows multiple peaks, in accordance with the literature; one has a shift of 286 cm^{-1}, and the other representing a strong acid site with a shift of 329 cm^{-1}. The integrated areas of O-H shifted CO signals allow for a comparison between the relative numbers of acid sites. Both SAPO-34 and SAPO-37 show significant quantities of acid sites, owing to a large proportion of isolated type II silicon species and similar silicon loadings. In contrast the silicon islanding in SAPO-41 and SAPO-5 results in fewer acid sites as expected (Table S4). Further insights on the acidic properties of these materials can be gained through ammonia-TPD, as a complementary tool to CO FT-IR (Figure 7 & Table S5). We note that while CO and NH_3 cannot assuredly interact with all the acid species present, they can interact with the majority, and any sites not accessible to

View Article Online
DOI: 10.1039/C8CY01770F

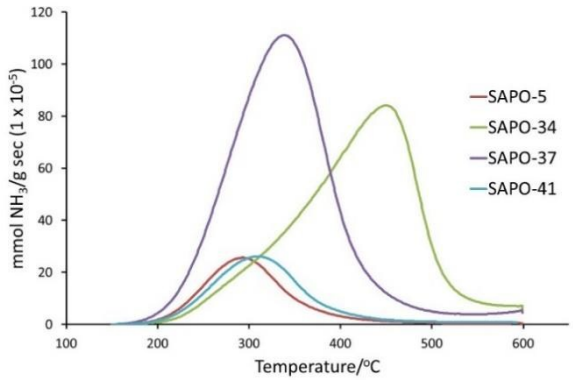

Figure 7 Quantifying total acidity and acid strength with NH_3-TPD.

these probes will not be of interest catalytically for the larger species employed. TPD data emphasizes the trends witnessed above, with SAPO-37 and SAPO-34 showing similar quantities of acid sites, yet SAPO-34 possessing significantly stronger acid sites (Table S5). In contrast the SAPO-5 and SAPO-41 species possess a much lower quantity of acid sites. Further, these sites are weaker strength acid sites than those present in SAPO-34. It follows that to generate significant quantities of Brønsted acidity within an AlPO framework, targeted type II substitution is required. Despite identical substitution processes, the strength of the acid sites generated is dependent on the specific framework topology, as seen in SAPO-37 and SAPO-34. The combination of silicon islanding and a reduced quantity of framework silicon leads to the formation of substantially fewer acid sites with weaker acidity in the SAPO-5 and SAPO-41 catalysts (Table 2 and S3).[58]

Despite providing information on the nature of all the acid sites present, neither CO, nor NH_3, are comparable in size to the cyclohexanone oxime substrate. Therefore, to gain a better understanding of the chemical potential for the Beckmann rearrangement process, a more discerning probe molecule is necessary. Here collidine is used as a probe to mimic the bulkier cyclohexanone oxime (Figures 8, 9, S8 and S9 and Table S6).[15] Once adsorbed, the amount of bound collidine was determined by quantifying the areas of the collidinium ν_{8a} and ν_{8b} signals (1637 and 1652 cm^{-1} respectively)[61] upon heating over a range of temperatures. Of the four samples, the larger-pore SAPO-37 catalyst was the only sample to show significant collidine uptake (0.41 mmol g^{-1}), with SAPO-5 showing only a slight affinity for collidine (0.05 mmol g^{-1}). The quantity of collidine absorbed by SAPO-41 and SAPO-34 was comparable, yet minimal (0.01 and 0.02 mmol g^{-1} respectively). These observations can be rationalized by the framework motifs and pore-geometries. The large-pore SAPO-37 (7.4 Å), permits the collidine probe access to the internal acid sites. However it is noted that only 44 % of the total acid sites (determined from NH_3-TPD, Table S7) were accessible to collidine, likely due to bound collidine blocking neighbouring acid sites. In contrast, only 30 % of the active sites in SAPO-5 are accessible, despite possessing similar-sized micropores (7.3 Å). This shows collidine is able to access the internal sites, however the 1D nature of the AlPO-5 (AFI) framework, makes it susceptible to pore-blockage, hindering access to some internal acid sites. Whereas the 3D intertwining micropores of SAPO-37 will not be affected to the same degree, allowing greater uptake. Further the silicon islanding of SAPO-5 (seen in ^{29}Si NMR) will lead to more site-blockage from interacting collidine molecules.[62,63] Finally the distinction in total collidine adsorption between the samples (0.41 mmol/g SAPO-37 and 0.05 mmol/g SAPO-5) mirrors the total number of acid sites present in both materials, as seen from NH_3-TPD (Figures 7 and Table S5).

The similar collidine uptake of the SAPO-34 and -41 catalysts, despite differing in both structural and physicochemical factors, is indicative of limited internal diffusion due to the smaller pores (Figure 1), therefore collidine is primarily adsorbing on the external surface, exclusively providing information on the catalytically available active sites. The similar uptake is indicative of the similar external surface areas between the two species (Table 1). It is emphasized that, while collidine is a comparable size to cyclohexanone, (more so than CO or NH_3), they are not identical, as such there may be differences in accessibility; though currently the total number of accessible sites follows the trend: SAPO-37 > SAPO-5 > SAPO-34 ≈ SAPO-41. The subject of active-site accessibility is fundamental in determining reaction kinetics and optimizing catalyst performance, particularly in the low-temperature Beckmann rearrangement.[15,65,66]

The collidine desorption temperatures differs in the larger-pore SAPO-37 and SAPO-5 compared to the smaller pore SAPO-34 and SAPO-41 (Figure 9 and Table S6). In SAPO-34 and -41 the majority of the collidine is desorbed between 150-300 °C, suggesting the available (external) acid sites are weaker acid sites. Such behaviour is typical of hydroxyl species, likely due to the Si-OH and P-OH groups seen via FT-IR (Figure 5). These species tend to be surface defect sites with little acidity, similar to silanols in zeolites, therefore would be readily accessible to collidine and catalytically active. In contrast the accessible active sites in SAPO-5 and SAPO-37 tend to desorb at higher temperatures, between 300-450 °C. This suggests the active

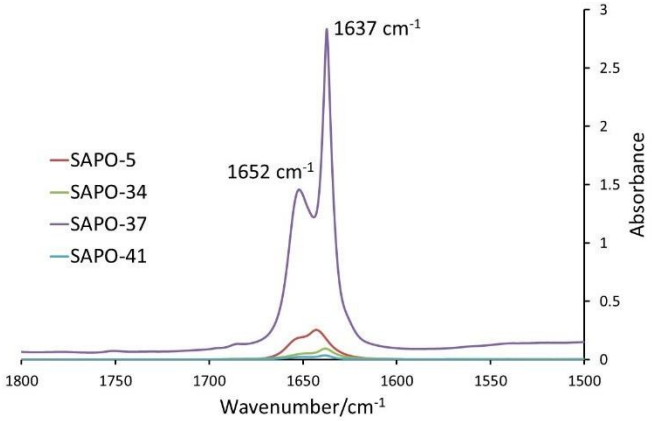

Figure 8 Collidine probed FT-IR spectra showing accessible acid sites after desorption at 150 °C.

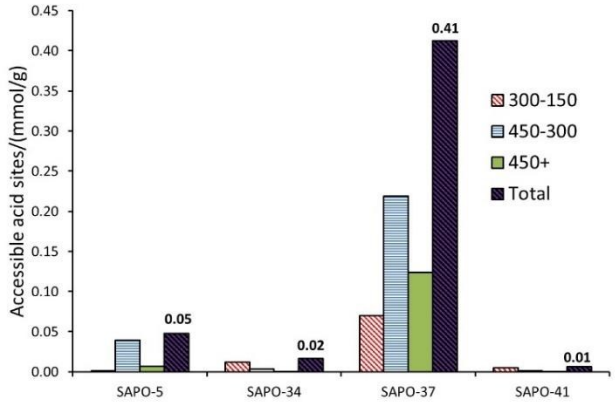

Figure 9 Quantitative analysis of accessible acid sites from collidine-probed FT-IR, grouping acid sites by the temperature at which collidine is desorbed, in °C.

sites which are accessible in SAPO-37 and SAPO-5 have a stronger interaction with collidine, and may be better suited for interacting with the cyclohexanone oxime reagent.

The four SAPO catalysts show distinct acidity trends, therefore the production of ε-caprolactam using these heterogeneous solid-acid nanoporous materials was investigated. Both their activity for the liquid (130 °C) and vapour-phase (≥ 300 °C) Beckmann rearrangement processes was evaluated. The liquid phase method, while traditionally less efficient, has the advantage of being less energy intensive, given the lower temperatures required.[12,25,26,67] It also offers prospects for studying interplay with the accessible active sites (as selectively probed by the collidine FT-IR) within the different framework topologies employed in this study. Under identical conditions significant differences in both activity and product specificity were observed between the four different frameworks.

Samples were taken after 7 hours, these conditions were chosen as systems showed no significant change in activity or product distribution after this time (Figures S10-S12), thus the reaction was deemed to be complete. Clear trends are evident in both conversion and selectivity for the liquid-phase process (Figure 10 & Table S8). We note that the overall activity of the catalysts does not immediately correlate with insights gained

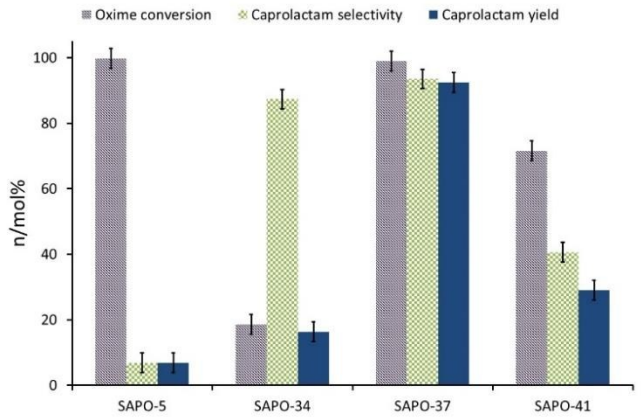

Figure 10 Catalytic data from the liquid-phase Beckmann rearrangement, emphasizing the influence of framework topology. Conditions: 130 °C, 7 hours, 20 ml benzonitrile (see ESI for further details).

(Figure 10 & Table S8). We note that the overall activity of the catalysts does not immediately correlate with insights gained from the nature and strength of all acid sites, or even the local silicon environment. Instead a more intuitive relationship exists between pore-size and catalytic activity, similar to the trend seen in the collidine-probed FT-IR data (Figures 9, 10, S8 and S9 and Table S6). This is reinforced by considering the production rate of caprolactam per mole of silicon dopant (Table S8). This finding suggests that acid site accessibility is a key metric for the liquid-phase Beckmann rearrangement. We note that while all species contain surface Si-OH and P-OH species (as seen in the FT-IR, Figure 6) there are significant variations in the catalytic activity, suggesting these weaker sites do not play a significant role in the catalysis.[68] As such our findings are further emphasized when also considering the activity of Zeolite-Y and ZSM-5 under similar conditions (Table S8).[15] It is seen that the FAU systems (SAPO-37 and Zeolite-Y) have the highest activity, due to the larger intertwining 3D micropores and FAU supercages, permitting access to the internal active sites, not hindering the formation of bulky transition states and allowing the ε-caprolactam product away to diffuse away. This prevents over-activation and coking, causing the improved catalytic performance of the two faujasitic species at low temperatures. However this shows the importance of having the appropriate acid sites, to form a recyclable, active catalyst (Table S9).

The 1D SAPO-5 material (pore-diameter of 7.3 Å, AFI), is more active than the SAPO-34 and -41 catalysts, due to the higher amount of available acid sites (Figure 9, Table S6). Interestingly our previous work on ZSM-5 (pore diameter of 5.4 Å, MFI) shows its catalytic performance lies between SAPO-41 and SAPO-34, in keeping with the trend in activity *versus* pore-size. Recently we have shown that cyclohexanone oxime is unable to diffuse into the ZSM-5 framework over the timescales observable using quasi-elastic neutron scattering.[15] But a significant body of evidence that suggests ZSM-5 catalyses the Beckmann rearrangement at the pore-mouths[12,69] It is highly likely that the improved lactam yield for ZSM-5 over SAPO-34 is due to the accessible pore-mouth acid sites of ZSM-5, which are more active than external surface sites of SAPO-34 (as probed through collidine FT-IR). Similarly the larger pores in SAPO-41, will allow the oxime to access a greater quantity of internal sites, than ZSM-5 and SAPO-34, explaining the improved activity. As despite the larger collidine probe being principally unable to access the SAPO-41 micropores, the smaller cyclohexanone oxime may still achieve limited diffusion.

To better understand the selectivity of the liquid Beckmann rearrangement we must consider the distribution of desorption temperatures within the collidine FT-IR data (Figure 10). Contrasting this data for SAPO-37, SAPO-5 and Zeolite-Y it is clear that the latter has a larger proportion of stronger acid sites (Figure 9, Table S6). These stronger sites are known to promote ring-opening reactions, and the formation of cyclohexanone, over caprolactam.[15] This suggests that not only is the diffusion into the faujasitic framework vital (for low-temperature acid catalysis) but promoting desirable acid sites, is crucial to facilitating high selectivities for ε-caprolactam. It has been shown in the literature[25,59] that the external silanol sites of

ZSM-5 are not as active under these conditions, and are also known to result in lower selectivity.[25,59] However stronger Brønsted acid sites around the pore-mouths have been shown to be selective for this reaction, but may not be as readily accessible as the weaker surface silanol sites.[25,59]

In the case SAPO-34 and -41, the accessible sites (available to collidine) were primarily weak acidic sites residing on the surface. Further, it is well-known that microporous materials are able to suppress the formation of ε-caprolactam, as the constricting micropores instead favour the formation of linear ring-opening products.[70] However reactions occurring inside the larger-pore SAPO-37, and on the external surface of SAPO-34, will not be sterically hindered; thereby promoting the formation of the caprolactam product. Our results strongly suggest that the external surface acid sites (as probed by collidine FT-IR) are ineffective for activating the oxime molecule under liquid-phase reaction conditions. Crucially, access to the internal micropores, that host the desirable acid sites, is therefore imperative for the liquid-phase approach, as reflected in the collidine adsorption studies (Figures 8, 9, S8 and S9 and Tables S6 and S7). However for a high yield of caprolactam to be achieved it is necessary that the active species be accessible, and of the correct strength, both of which are an inherent feature of the framework topology.[15]

The vapour-phase process, while requiring higher temperatures, utilises a cheaper solvent (ethanol) for industrial applicability, often leading to greater catalyst efficiencies and lifetime.[7,9-13] We compare our liquid-phase findings with the vapour-phase findings to gain a more holistic understanding of the Beckmann process, while a range of conditions were investigated, including temperature (Figures 11, S13 and S14), time on stream (Figure S15) and WHSV (Figure S16 and S17), a common set of conditions were chosen to optimise performance and limit deactivation for meaningful comparisons based on the characterisation of the 'fresh' samples. While direct comparisons cannot be made due to the differing experimental liquid and vapour-phase set-ups, there is sufficient understanding to draw useful conclusions from the different catalysts. Given the industrial implementation of the medium-pore HZSM-5 catalyst (5.4 Å), it is likely internal diffusion is not as significant in the vapour-phase, compared to the liquid-phase process.[15,26,55] We studied the vapour-phase process over a range of temperatures, in order to compare our findings with current literature methods.[7,9-13] At first glance, at the lowest temperature (300 °C) the trend in caprolactam yield, for SAPOs, resembles that of the liquid phase process (Figures 10, 11, S13 and S14). The larger-pore SAPO-37 displays better catalytic performance when compared with SAPO-5 and SAPO-41, however is not as efficient, due to the threefold-higher silicon loading (Figure S18) in SAPO-37. The smaller pore-aperture of the SAPO-34 catalyst is comparatively ineffective at 300 °C. Analogous arguments can therefore be inferred with regards to diffusion kinetics and the nature of the specific active

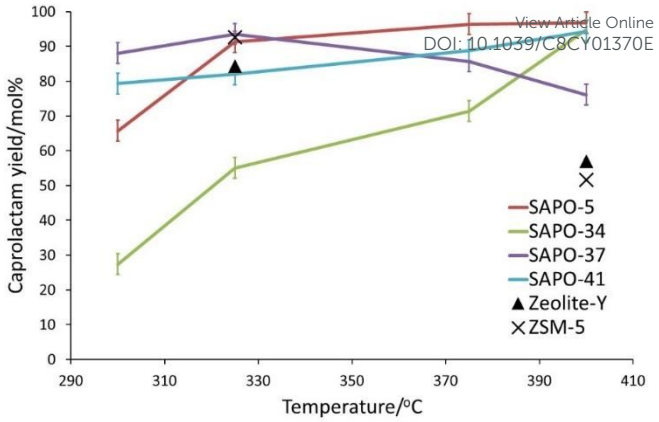

Figure 11 The influence of framework architecture on the vapour-phase Beckmann rearrangement. Conditions: Liquid feed of 10 wt% cyclohexanone oxime in ethanol, WHSV of 0.4 hr^{-1}, 33.3 ml of He carrier gas, 1 hr on stream.

sites under these conditions. However, it should be noted that, despite being a poor liquid-phase catalyst, ZSM-5 shows excellent activity at 325 °C (mirroring SAPO-37) which is not in is observed. The small-pore SAPO-34 catalyst produces a higher lactam yields similar to SAPO-41 and SAPO-5, despite SAPO-41 and SAPO-5 consistently being the most efficient catalysts per mol of silicon dopant (Figure S18). The improved activity of SAPO-34 suggests that the neutral surface acid sites have been modified resulting in enhanced catalytic performance. Despite marked differences in diffusion occurring between the 130 °C liquid phase and 400 °C vapour phase processes, internal diffusion of cyclohexanone oxime is still highly unlikely in SAPO-34. However, given the increased activity, it must be concluded that the desirable (modulated) active sites are located on the surface or at the pore-mouth of the SAPO-34 catalyst. In this case, the higher temperatures (400 °C) activate the surface sites, thereby enabling a greater proportion of the desirable surface sites to catalyse the Beckmann rearrangement reaction. Modulation of surface acid sites[2,30] at these temperatures occurs to a greater extent in SAPO-5 and -34, accounting for a complete reversal in catalytic performance. A decrease in lactam yield at 400 °C was observed in Zeolite-Y, ZSM-5 and SAPO-37 (Figure 11). Despite seeing increased conversion at higher temperatures (Figure S13), the selectivity decreased (Figure S14). This is believed to be due to the formation of heavier by-products, that desorb at higher temperatures, and also due to the formation of ring-opening products, which lowered the selectivity of Zeolite-Y as the WHSV increased (Figure S16), however at higher WHSV only cyclohexanone was seen as a by-product for SAPO-37 (Figure S17).[73,74] The fact that are catalytically significant. The main difference comes in lactam selectivity (Figure S14): the weaker acid sites of SAPO-5 and -34 are now the most selective, suggesting that even at the higher temperatures (400 °C), the weaker sites are not able to instigate further reactions of the lactam, or ring-opening, unlike the SAPO-37, Zeolite-Y and ZSM-5.[73,74] As such, a gradual

View Article Online
DOI: 10.1039/C8CY01370E

Table 3 Combined catalytic analysis normalised per mole of silicon dopant and by total acidity.

Liquid Phase – 130 °C

Material	Conversion /mol%	Selectivity /mol%	Yield /mol%	TON (Si content) /(mol/mol)[a]	TON (Total acidity) /(mol/mol)[b]	Lactam Production (Si content) /(mol/mol)[c]	Lactam Production (Total acidity) /(mol/mol)[d]
SAPO-5	99.8	6.8	6.8	17.7	51.3	1.2	3.5
SAPO-34	18.6	87.3	16.2	1.4	2.0	0.2	0.3
SAPO-37	98.9	93.5	92.5	8.2	9.4	7.6	8.7
SAPO-41	71.6	40.6	29.1	16.2	31.2	4.7	9.1

Vapour Phase – 300 °C

Material	Conversion /mol%	Selectivity /mol%	Yield /mol%	TOF (Si content) /(mol/mol.hr)[e]	TOF (Total acidity) /(mol/mol.hr)[f]	Lactam Production Rate (Si content) /(mol/mol.hr)[g]	Lactam Production Rate (Total acidity) /(mol/mol)[h]
SAPO-5	66.8	98.3	65.7	4.7	13.7	4.7	13.5
SAPO-34	36.3	75.5	27.4	1.1	1.6	0.8	1.2
SAPO-37	92.6	95.1	88.1	3.1	3.5	2.9	3.4
SAPO-41	97.2	81.6	79.3	8.8	16.9	7.2	13.8

Vapour Phase – 400 °C

Material	Conversion /mol%	Selectivity /mol%	Yield /mol%	TOF (Si content) /(mol/mol.hr)[e]	TOF (Total acidity) /(mol/mol.hr)[f]	Lactam Production Rate (Si content) /(mol/mol.hr)[g]	Lactam Production Rate (Total acidity) /(mol/mol)[h]
SAPO-5	100.0	96.8	96.8	7.1	20.6	6.9	19.9
SAPO-34	100.0	94.7	94.7	2.9	4.3	2.8	4.1
SAPO-37	100.0	76.1	76.1	3.3	3.8	2.5	2.9
SAPO-41	100.0	94.3	94.3	9.0	17.4	8.5	16.4

a) mols of cyclohexanone oxime consumed, normalised by mols of silicon dopant, as determined by Si content in catalyst. b) mols of cyclohexanone oxime consumed, normalised by mols of total acid sites present, as determined by NH_3-TPD. c) mols of Caprolactam produced, normalised by mols of silicon dopant, as determined by Si content in catalyst. d) mols of Caprolactam produced, normalised by mols of total acid sites present, as determined by NH_3-TPD. e) TON (Si content) per hr. f) TON (Total acidity) per hr. g) Lactam Production (Si content) per hr. h) Lactam production (Total acidity) per hr.

progression in catalytic behaviour is noted with increasing temperatures, further vindicating the modulation of the acid site characteristics across the different catalysts.It is clear, that while the Beckmann rearrangement mechanism is well known (Figure S19), differences in catalytic behaviour can be observed, depending on the reaction temperature. While diffusion plays a major role in influencing the reaction rate in the liquid-phase, the higher temperatures of the vapour-phase activate the acid sites at the external surface and pore-mouth of the catalysts. It is therefore highly likely that the liquid-phase Beckmann rearrangement primarily occurs on the more desirable internal acid sites, whilst the vapour-phase process can implicate the modulated external surface acid sites (and acid sites at the pore-extremities), as observed in other acid-catalysed transformations.[15,23,66] This is emphasised in our catalytic findings (Table 3) where SAPO-37 is more effective for caprolactam production in the liquid-phase, highlighting the importance of accessibility to the desired internal acid sites. In contrast, in the vapour phase we see that the SAPO-5 and SAPO-41 species are most effective and efficient catalysts for lactam production, emphasising the influence of desirable surface acid sites at higher temperatures.

Conclusions

The influence of zeotype framework topology has been explored with reference to silicon-substitution mechanisms, which concomitantly modulates the nature and type of desirable active sites, in the Beckmann rearrangement of cyclohexanone oxime. By doping silicon into an AlPO framework (generating a SAPO species) one can induce an array of diverse solid-acid active centres within the nanoporous framework. The precise nature, location and strength of these active sites has been explored using a combination of structural, physico-chemical and *in situ* spectroscopy, which have been designed to correlate the nature of the Brønsted acid active sites to the framework-specific substitution mechanism. The influence of the specific framework topology and its influence in facilitating desirable interactions with internal and external solid-acid centres has been probed in the liquid- and gas-phase Beckmann rearrangement of cyclohexanone oxime. The location and strength of such solid-acid sites within different zeolite and zeotype topologies is crucial in the tunability of catalytic properties at low-temperatures. Furthermore, the differences in catalytic profiles have been aligned with the multi-technique

characterization study to determine modulation characteristics on active centres located within microporous solids. These studies also revealed contrasting catalytic behaviour between the liquid and vapour-phase processes, which lead to unique mechanistic insights that can be derived on the basis of site-specific interactions of the active sites. The structure-property correlations derived from this study suggest that accessibility and acid site strength determined by collidine FT-IR, are both key metrics for achieving high lactam yields, and are both functions of the specific framework topology. This therefore provides a distinct insight into the design of solid-acid active centres for low-temperature acid-catalysed transformations, affording fundamental perspectives on the rational design of targeted solid-acid catalysts.[75]

Conflicts of interest

There are no conflicts to declare.

Acknowledgements

MEP was sponsored by Honeywell LLC and RB was funded by University of Southampton.

Notes and references

1 R. Raja, M. E. Potter and S. H. Newland, *Chem. Commun.*, 2014, **50**, 5940.
2 E. Gianotti, M. Manzoli, M. E. Potter, V. N. Shetti, D. Sun, J. Paterson, T. M. Mezza, A. Levy and R. Raja, *Chem. Sci.*, 2014, **5**, 1810.
3 J. M. Thomas, R. Raja and D. W. Lewis, *Angew. Chem. Int. Ed.*, 2005, **44**, 6456.
4 X. F. Yang, A. Wang, B. Qiao, J. Li, J. Liu and T. Zhang, *Acc. Chem. Res.*, 2013, **46**, 1740.
5 "Nylon – A global strategic business report" Global industry analysts inc., 2010**.**
6 G. Bellussi and C. Perego, *CATTECH*, 2000, **4**, 4.
7 A. Thangaraj, S. Sivasanker and P. Ratnasamy, *J. Catal.*, 1992, **137**, 252.
8 M. Mantegazza and G. Petrini, *US Patent*, 1996, US 5498793 A.
9 H. Kajikuri, M. Kitamura and Y. Higashio, *US Patent*, 1994, US 5304643 A.
10 G. P. Heitmann, G. Dahlhoff and W. F. Hoelderich, *J. Catal.*, 1999, **186**, 12.
11 W. C. Li, A. Lu, R. Palkovits, W. Schmidt, B. Spliethoff and F. Schuth, *J. Am. Chem. Soc.*, 2005, **127**, 12595.
12 A. B. Fernandez, I. Lezcano-Gonzalez, M. Boronat, T. Blasco and A. Corma, *J. Catal.*, 2007, **249**, 116.
13 K. Na, C. Jo, J. Kim, K. Cho, J. Jung, Y. Seo, R. J. Messinger, B. F. Chmelka and R. Ryoo, *Science*, 2011, **333**, 328.
14 A. B. Levy, R. Raja and M. E. Potter, *US Patent*, 2013, US 20130109851 A1.
15 M. E. Potter, A. J. O'Malley, S. Chapman, J. Kezina, S. H. Newland, I. P. Silverwood, S. Mukhopadhyay, M. Carravetta, T. M. Mezza, S. F. Parker, C. R. A. Catlow and R. Raja, *ACS Catal.*, 2017, **7**, 2926.
16 S. Wilson and P. Barger, *Micropor. Mesopor. Mater.*, 1999, **29**, 117.
17 B. P. C. Hereijgers, F. Bleken, N. H. Nilsen, S. Svelle, K. P. Lilerud, M. Bjorgen, B. M. Weckhuysen and U. Olsbye, *J. Catal.*, 2009, **264**, 77.
18 P. T. Barger, *US Patent*, 1992, US5095163 A.
19 I. Miletto, G. Paul, S. Chapman, G. Gatti, L. Marchese, R. Raja and E. Gianotti, *Chem. Eur. J.*, 2017, **23**, 9952.
20 M. Anilkumar and W. F. Hoelderich, *J. Catal.*, 2012, **293**, 76.
21 J. Kim, W. Park and R. Ryoo, *ACS Catal.*, 2011, **1**, 337.
22 E. G. Vaschetto, S. G. Casuscelli and G. A. Eimer, *Micropor. Mesopor. Mater.*, 2016, **221**, 175.
23 Y. Chu, P. Ji, X. Yi, S. Li, P. Wu, A. Zheng and A. Deng, *Catal. Sci. Technol.*, 2015, **5**, 3675.
24 M. E. Potter, D. Sun and R. Raja, *Catal. Sci. Technol.*, 2016, **6**, 2616.
25 M. A. Camblor, A. Corma, H. Garcia, V. Semmer-Herledan and S. Valencia, *J. Catal.*, 1998, **177**, 267.
26 C. Ngamcharussrivichai, P. Wu and T. Tatsumi, *J. Catal.*, 2004, **227**, 448.
27 M. Hartmann and L. Kevan, *Chem. Rev.*, 1999, **99**, 635.
28 R. M. Leithall, V. N. Shetti, S. Maurelli, M. Chiesa, E. Gianotti and R. Raja, *J. Am. Chem. Soc.*, 2013, **135**, 2915.
29 L. Gomez-Hortiguela, F. Cora, G. Sankar, C. M. Zicovich-Wilson and C. R. A. Catlow, *Chem. Eur. J.*, 2010, **16**, 13638.
30 M. E. Potter, D. Sun, E. Gianotti, M. Manzoli and R. Raja, *Phys. Chem. Chem. Phys.*, 2013, **15**, 13288.
31 J. Paterson, M. E. Potter, E. Gianotti and R. Raja, *Chem. Commun.*, 2010, **47**, 517.
32 J. M. Thomas, R. Raja and D. W. Lewis, *Angew. Chem. Int. Ed.*, 2005, **44**, 6456.
33 M. E. Potter, M. E. Cholerton, J. Kezina, R. Bounds, M. Carravetta, M. Manzoli, E. Gianotti, M. Lefenfeld and R. Raja, *ACS Catal.*, 2014, **4**, 4161.
34 S. H. Newland, W. Sinkler, T. M. Mezza, S. R. Bare, M. Carravetta, I. Haies, A. Levy, S. Keenan, R. Raja, *ACS Catal.*, 2015, **5**, 6587.
35 P. Meriaudeau, V. A. Taun, V. T. Ngheim, S. Y. Lai, L. N. Hung and C. Naccache, *J. Catal.* 1997, **169**, 55.
36 M. Dugal, G. Sankar, R. Raja and J. M. Thomas, *Angew. Chem. Int. Ed.*, 2000, **39**, 2310.
37 J. M. Thomas, R. Raja, G. Sankar and R. G. Bell, *Nature*, 1999, **398**, 227.
38 J. C. Groen, W. Zhu, S. Brouwer, S. J. Huynink, F. Kapteijn, J. A. Moulijn and J. Perez-Ramirez, *J. Am. Chem. Soc.*, 2007, **129**, 355.
39 G. Sastre, D. W. Lewis and C. R. A. Catlow, *J. Phys. Chem. B*, 1997, **101**, 5249.
40 G. Sastre, D. W. Lewis and C. R. A. Catlow, *J. Phys. Chem.*, 1996, **100**, 6722.
41 "Collection of simulated XRD powder patterns for zeolites" M. M. J. Treacy and J. B. Higgins, Elsevier, 5th edition.
42 M. E. Potter, A. J. Paterson and R. Raja, *ACS Catal.*, 2012, **2**, 2446.
43 B. M. Lok, C. A. Messina, R. L. Patton, R. T. Gajek, T. R. Cannan and E. M. Flanigen, *J. Am. Chem. Soc.*, 1984, **106**, 6092.
44 M. Behrens, F. Studt, I. Kasatkin, S. Kuhl, M. Havecker, F. Abild-Pedersen, S. Zander, F. Girgsdies, P. Kurr, B. L. Kniep, M. Tovar, R. W. Fischer, J. K. Norskov and R. Schlogl, *Science*, 2012, **336**, 893.
45 S. Maurelli, M. Chiesa, E. Giamello, R. M. Leithall and R. Raja, *Chem. Commun.*, 2012, **48**, 8700.
46 S. A. Bartlett, P. P. Wells, M. Nachtegaal, A. J. Dent, G. Cibin, G. Reid, J. Evans and M. Tromp, *J. Catal.*, 2011, **284**, 247.
47 E. Gianotti, V. N. Shetti, M. Manzoli, J. A. L. Blaine, W. C. Pearl Jr., R. D. Adams, S. Coluccia and R. Raja, *Chem. Eur. J.*, 2010, **16**, 8202.
48 D. I. Enache, J. K. Edwards, P. Landon, B. Solsona-Espiru, A. F. Carley, A. A. Herzing, M. Watanabe, C. J. Kiely, D. W. Knight and G. J. Hutchings, *Science*, 2006, **311**, 362.

View Article Online
DOI: 10.1039/C8CY01370E

49 W. Shen, X. Li, Y. Wei, P. Tian, F. Deng, X. Han and X. Bao, *Micropor. Mesopor. Mater.*, 2012, **158**, 19.
50 E. Lippmaa, A. Samoson and M. Magi, *J. Am. Chem. Soc.*, 1986, **108**, 1730.
51 C. S. Blackwell and R. L. Patton, *J. Phys. Chem.*, 1984, **88**, 6135.
52 C. S. Blackwell and R. L. Patton, *J. Phys. Chem.*, 1988, **92**, 3965.
53 L. Marchese, J. Chen, J. M. Thomas, S. Coluccia and A. Zecchina, *J. Phys. Chem.*, 1994, **98**, 13350.
54 M. A. Makarova, A. F. Ojo, K. Karim, M. Hunger and J. Dwyer, *J. Phys. Chem.*, 1994, **98**, 3619.
55 S. Bordiga, L. Regli, C. Lamberti, A. Zecchina, M. Jorgen and K. P. Lillerud, *J. Phys. Chem. B*, 2005, **109**, 7724.
56 S. Bordiga, C. Lamberti, F. Geobaldo, A. Zecchina, G. Turnes Palomino and C. Otero Arean, *Langmuir*, 1995, **11**, 527.
57 O. Cairon, T. Chevreau and J. C. Lavalley, *J. Chem. Soc., Faraday Trans.*, 1988, **94**, 3039.
58 K. G. V. A. Martins, G. Berlier, C. Bisio, S. Collucia, H. O. Pastore and L. Marchese, *J. Phys. Chem. C*, 2008, **112**, 7193.
59 K. Chakarova and K. Hadjiivanov, *J. Phys. Chem. C*, 2011, **115**, 4806.
60 G. E. Ewing, *J. Chem. Phys.*, 1962, **37**, 2250.
61 G. Paul, C. Bisio, I. Braschi, M. Cossi, G. Gatti, E. Gianotti and L. Marchese, *Chem. Soc. Rev.*, 2018, **47**, 5684.
62 F. Thibault-Starzyk, I. Stan, S. Abello, A. Bonilla, K. Thomas, C. Fernandez, J. P. Gilson and J. Perez-Ramirez, *J. Catal.*, 2009, **264**, 11.
63 M. S. Holm, S. Svelle, F. Joensen, P. Beato, C. H. Christensen, S. Bordiga and M. Bjorgen, *Appl. Catal. A: Gen.*, 2009, **356**, 23-30.
64 F. Thibault-Starzyk, A. Vimont and J. P. Gilson, *Catal. Today*, 2001, **70**, 227.
65 C. Flego and L. Dalloro, *Micropor. Mesopor. Mater.*, 2003, **60**, 263.
66 A. B. Fernandez, A. Marinas, T. Blasco, V. Fornes and A. Corma, *J. Catal.*, 2006, **243**, 270.
67 M. Linares, C. Vargas, A. Garcia, C. Ochoa-Hernandez, J. Cejka, R. A. Garcia-Munoz and D. P. Serrano, *Catal. Sci. Technol.*, 2017, **7**, 181.
68 J. Chen, J. M. Thomas and G. Sankar, *J. Chem. Soc. Faraday Trans.*, 1994, **90**, 3455.
69 V. R. Reddy-Marthala, S. Rabl, J. Huang, S. A. S. Rezai, B. Thomas and M. Hunger, *J. Catal.*, 2008, **257**, 134.
70 T. Takahashi, M. N. A. Nasution and T. Kai, *Appl. Catal. A: Gen.*, 2001, **210**, 339.
71 A. B. Fernandez, I. Lezcano-Gonzalez, M. Boronat, T. Blasco and A. Corma, *Phys. Chem. Chem. Phys.*, 2009, **11**, 5134.
72 V. R. Reddy-Marthala, J. Frey and M. Hunger, *Catal. Lett.*, 2010, **135**, 91.
73 P. S. Singh, S. G. Bandyopadhyay, S. G. Hegde and B. S. Rao, *Appl. Catal. A: Gen*, 1996, **136**, 249.
74 L. Forni, G. Fornasari, G. Giordano, C. Lucarelli, A. Katovic, F. Trifiro, C. Perri and J. B. Nagy, *Phys. Chem. Chem. Phys.*, 2004, **6**, 1842.
75 M. Lefenfeld, R. Raja, A. J. Paterson and M. E. Potter, *US Patent*, 2010, US 20100249476.

View Article Online
DOI: 10.1039/C8CY01370E

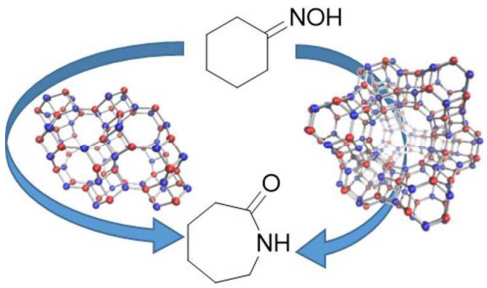

Framework topology and the acid sites significantly influence the Beckmann rearrangement, affecting the design of solid-acid catalysts.